

Stochastic Chern number from interactions and light response

Philipp W. Klein¹, Adolfo G. Grushin², and Karyn Le Hur¹

¹CPHT, CNRS, Ecole Polytechnique, Institut Polytechnique de Paris, Route de Saclay, 91128 Palaiseau, France and

²Institut Néel, CNRS and Université Grenoble Alpes, Grenoble, France

(Dated: December 21, 2024)

We develop a stochastic description of the topology in an interacting Chern insulator. Electron-electron interactions can produce a substantial number of particle-hole pairs above the band gap, which leads us to propose an interacting measure of the topology which we refer to as a “stochastic Chern number”. We confirm the Mott transition’s first-order nature in the interacting quantum anomalous Hall effect on the honeycomb geometry, from a mean-field topological variational approach, supported by density matrix renormalization group results. We make predictions for circular dichroism of light, and build an analogy between interaction-induced particle-hole pairs and temperature effects. Our stochastic approach is physically intuitive, computationally easy to implement and leads the way to further studies of interaction effects in Chern insulators.

Introduction - Topological phases of matter have attracted a lot of interest in the last years, including generalizations of the quantum Hall effect [1] to the Haldane model on the honeycomb lattice [2]. This gives rise to the quantum anomalous Hall effect which has been realized in quantum materials [3], graphene [4], photonic systems [5–10] and cold atoms in optical lattices [11, 12]. The occurrence of an insulating bulk and a protected chiral edge mode can be understood through a quantized topological number, the Chern number, assuming non-interacting particles. These systems at half-filling then behave as Chern insulators (CI). While some progress has been made in the description of interacting Chern systems, in the bosonic case [13, 14], and both for spinless [13, 15–17] and spinfull [18–22] fermions, and more generally in the description of interacting topological systems [23], several central questions remain open. In this Letter, we introduce a many-body description for interacting CIs, taking into account interaction-induced particle-hole pairs and describing Mott physics at half-filling.

To describe the effect of particle-hole pairs in the Haldane model on the honeycomb lattice with a nearest-neighbor interaction, we introduce a Hubbard-Stratonovitch transformation to re-write the quartic fermionic interaction as Gaussian variables [24], referring to stochastic variables. One stochastic variable can be identified as a Semenoff mass [25], which will produce a sign flip of the mass term at one Dirac point only at the Mott transition. Within this approach, there is a direct relation between the creation of particle-hole pairs above the band gap due to interaction effects and fluctuations of this stochastic variable around its mean value. By analogy to the studies of the two-dimensional Hubbard model [26], other variables dressing the kinetic term and referring to the particle-hole channel, will also play an important role. This particle-hole channel will produce a jump of the Charge Density Wave (CDW) order parameter at the Mott transition, already at a mean-field level from a variational approach, in agreement with infinite density matrix renormalization group (iDMRG) results.

We are astonished that this particle-hole channel which provides a physical insight behind the Mott transition’s first-order nature, has not been introduced before. The phase transition was previously shown to be first-order from exact diagonalization [13, 15]. We also analyse the phase transition using a Ginzburg-Landau approach [27].

Furthermore, circular dichroism of light is related to the quantized Chern number [28, 29] for the non-interacting Haldane model. Shining light induces a population of the states in the upper band, above the band gap. The associated depletion rates depend on the orientation of the circular drive. The Chern number is encoded in the difference of rates with opposite orientation. Through a mathematical formulation on the Bloch sphere, we show that the topology of the system is already described by the depletion rates that occur at the Dirac points of the Brillouin zone. Then, we consider interaction effects that contribute to the formation of particle-hole pairs and thereby stochastically change the Chern number as defined through the circular dichroism of light. We define the stochastic Chern number through an average of the Chern number on the ensemble of stochastic variables, which agrees with the quantized topological invariant for very weak interactions. Finally, we study how the stochastic topological number is linked to the finite-temperature Chern number [30].

The model - We consider the model Hamiltonian $\mathcal{H} = \mathcal{H}_0 + \mathcal{H}_V$, where \mathcal{H}_0 is the Haldane honeycomb model for spinless fermions at half-filling [2] and \mathcal{H}_V is the nearest neighbor interaction

$$\begin{aligned}\mathcal{H}_0 &= - \sum_{\langle i,j \rangle} t_1 c_i^\dagger c_j - \sum_{\langle\langle i,j \rangle\rangle} t_2 e^{\pm i\Phi} c_i^\dagger c_j \\ \mathcal{H}_V &= V \sum_{\langle i,j \rangle} (n_i - 1/2) (n_j - 1/2).\end{aligned}\quad (1)$$

Here, t_1 represents the nearest-neighbor hopping strength which we set to unity hereafter ($t_1 = 1$). Furthermore, $t_2 e^{\pm i\Phi}$ represents the next-nearest neighbor hopping term where we fix the Peierls phase to $\Phi = \pi/2$,

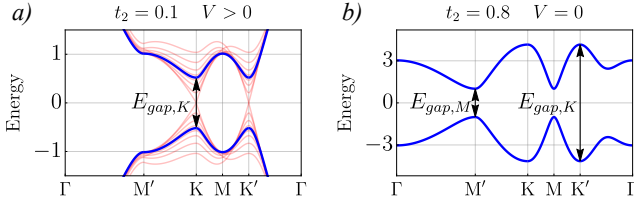


FIG. 1. (color online) (a) Band structure (blue pair of bands) for small $t_2 < 0.2$ with $t_1 = 1$. The low energy physics is centered around the Dirac points, where the stochastic approach applies. If we allow for fluctuations at $V > 0$, the sampling of ϕ^z corresponds to the creation of quasi states that change the band gap at the K and K' points. (b) Haldane band structure for large $t_2 > 0.2$ such that the low energy regime is located at the M-points.

for simplicity. Here, the positive (negative) sign refers to (counter-) clockwise hopping [31].

Previous studies [16, 17] have suggested that at a mean field level the quartic interaction term can be decoupled into a CDW order parameter which then acts as a staggered potential in sublattice space on \mathcal{H}_0 . A straightforward approach, proposed in Ref. [16], would be to rewrite \mathcal{H}_V exactly as $\mathcal{H}_V = \frac{V}{4} \sum_{\langle i,j \rangle} (n_i - n_j)^2$ in order to find a simple mean-field theory for the CDW order. Crucially however, this ansatz does not take into account the fact that the correlator $\langle c_i^\dagger c_j \rangle$, referring to the particle-hole channel [26], is finite in two-dimensional Hubbard models and therefore contributes to the interaction energy $\langle c_i^\dagger c_i c_j^\dagger c_j \rangle$. Hence, a valid decoupling scheme involving particle-hole channels has not been considered previously for interacting topological phases [16, 17]. When particle-hole channels are not included, one finds the Mott phase transition to be second-order [16].

A mean-field ansatz can be derived by rewriting the quartic term exactly as $c_i^\dagger c_i c_j^\dagger c_j = \sum_r \eta_r (c_i^\dagger \sigma_r^z c_j)^2$ where σ^r are the Pauli matrices acting on sublattice space, and r represents $(0, x, y, z)$. The coefficients η_r need to be chosen such that they fulfill the three conditions $\eta_0 = -\eta_z$, and $\eta_x = \eta_y$, as well as $1/4 = \eta_0 - \eta_x$. In general, the right choice of the η_r can only be systematically computed within a variational mean-field theory. Such an ansatz aims to minimize the energy of the full, original Hamiltonian $\langle \mathcal{H} \rangle$ with respect to the ground state of some trial Hamiltonian [31]. We find that the choice $\eta_0 = -\eta_{x,y,z} = \frac{1}{8}$ minimizes the energy.

We can then write down the partition function and action for the Hamiltonian \mathcal{H} and decouple the quartic interaction by performing a Hubbard-Stratonovich transformation [24, 32] for each r , so e.g. for $r \in (x, y, z)$ as $e^{\frac{V}{8} \sum_{i,p} (c_i^\dagger \sigma_r^z c_{i+p})^2} = \int \mathcal{D}\phi^r e^{-\sum_{i,p} 2V(\phi_{i+p/2}^r)^2 + V\phi_{i+p/2}^r (c_i^\dagger \sigma_r^z c_{i+p})}$ where i denotes a unit cell, $p \in (x, y, z)$, and we introduced an auxiliary field $\phi_{i+p/2}^r$ on each link between lattice sites i (sublattice A) and $i+p$ (sublattice B). The auxiliary-field variables are time-independent. Although we choose

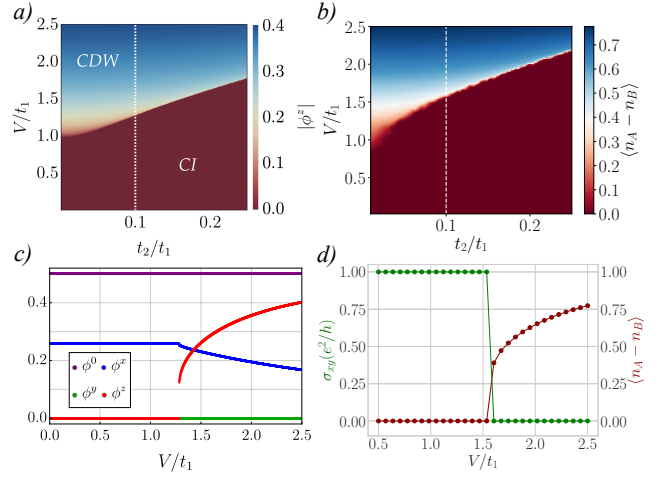


FIG. 2. (color online) (a) $V - t_2$ mean field phase diagram from the method. The transition marks the condensation of the CDW order parameter ϕ^z . (b) Same phase diagram obtained with iDMRG. (c) Absolute value of the self-consistent ϕ^r variable as a function of V for $t_2 = 0.1$. (d) Hall conductivity and $\langle n_A - n_B \rangle$ from iDMRG.

a decoupling ansatz similar to that of a quantum Monte Carlo approach [33], we do not experience the typical sign problem present in the interacting Haldane model since we do not sample the auxiliary fields in imaginary time.

After switching to Fourier space, we aim to build an effective model at the Dirac points. We keep the leading scattering contribution around each Dirac point. Finally, we derive the effective mean-field Hamiltonian $\mathcal{H}_{\text{mf}} = \sum_{\mathbf{k}} \Psi_{\mathbf{k}}^\dagger \mathcal{H}_{\text{mf}}^{\mathbf{k}} \Psi_{\mathbf{k}}$, where $\Psi_{\mathbf{k}}^\dagger = (c_{\mathbf{k}A}^\dagger, c_{\mathbf{k}B}^\dagger)$ is the spinor basis acting on sublattice A and sublattice B respectively, for each wavevector \mathbf{k} and

$$\mathcal{H}_{\text{mf}}^{\mathbf{k}} = \begin{pmatrix} \gamma(\mathbf{k}) - 3V(\phi^0 + \frac{1}{2}) & -g(\mathbf{k}) \\ -g^*(\mathbf{k}) & -\gamma(\mathbf{k}) - 3V(\phi^0 + \frac{1}{2}) \end{pmatrix} \quad (2)$$

is the Hamiltonian density. We have introduced the functions $\gamma(\mathbf{k}) = 3V\phi^z - 2t_2 \sum_p \sin(\mathbf{k} \cdot \mathbf{b}_p)$, and $g(\mathbf{k}) = [t_1 - V(\phi^x + i\phi^y)] \sum_p (\cos(\mathbf{k} \cdot \mathbf{a}_p) - i \sin(\mathbf{k} \cdot \mathbf{a}_p))$. The vectors \mathbf{a}_p and \mathbf{b}_p are the nearest and next-nearest neighbor displacements, respectively [31]. The field ϕ^0 can be absorbed in the chemical potential and will be fixed to $\phi^0 = -1/2$ at half-filling. Furthermore, the field ϕ^z changes sign in sublattice space and therefore plays the role of a staggered chemical potential. On the one hand, it measures the particle density difference between sublattices A and B, and captures CDW order. Furthermore, it acts as a Semenoff mass term [25] on the Haldane model and therefore controls the Chern number of the system [2]. Finally, the particle-hole channels ϕ^x and ϕ^y dress the nearest-neighbor hopping term t_1 . By symmetry, we find that $\phi^y = 0$ for all the values of V (in agreement with the numerical results below) and the other stochastic variables ϕ^x and ϕ^z are real.

In Fig. 2a), we present the two-dimensional $t_2 - V$

phase diagram obtained with a variational approach on the mean-field theory and additional information on the method can be found in the Supplementary Material [31]. We confirm the presence of two phases [13, 14], a CI phase with a perfectly quantized Chern number and a Mott or CDW phase. The self-consistent equations for the auxiliary mean-field order parameters read $\phi^r = -\frac{1}{2}\langle c_i^\dagger \sigma_{ij}^r c_j \rangle$. Fig. 2c) shows the numerical solution of the mean field equations for $t_2 = 0.1$. The jump in the CDW order parameter ϕ^z indicates the first-order phase transition. In the Supplemental Material [31], we also show the evolution of the CDW jump as a function of t_2 , and we develop a Ginzburg-Landau analysis which supports the first-order nature of the transition.

iDMRG results - We have compared our mean field calculations with simulations using the infinite density matrix renormalization group (iDMRG) by means of the python package TENPY [34], written in the language of matrix product states. This numerical method calculates the ground-state of the model (1) in the infinite cylinder geometry, as well as the expectation of the CDW order parameter, $\langle n_A - n_B \rangle$, the Hall conductivity σ_{xy} , the correlation length ξ and the entanglement entropy S . The bond dimension χ is a measure of the maximum number of states kept by the algorithm, and sets the accuracy of the calculation. We have performed calculations up to $\chi = 1200$ for cylinder circumferences of $L_y = 6, 12$ sites observing that our results show good convergence for bond dimensions as low as $\chi \gtrsim 200$, consistent with previous iDMRG calculations [35] (see [31]). The phase diagram for $\chi = 200$ and $L_y = 6$ is shown in Fig. 2b). It shows the same phases as our mean-field calculation, yet mean-field mildly underestimates the critical V phase boundary compared to iDMRG. In Fig. 2d) we show the CDW order parameter and the Hall conductivity along a cut at $t_2/t_1 = 0.1$, which show a discontinuity along the transition for all χ s. These discontinuities are typical of a first-order phase transition, further supported by the saturation of the entanglement entropy at the transition as a function of correlation length (see [31]). Comparing iDMRG results with the mean-field variational approach, our findings agree as long as the smallest band gap (relevant energy scale for CDW order) is located at the K-points (relevant for topology), which is the case for $t_2 \leq 0.2$ [31]. Therefore, we focus on this parameter regime.

Circular dichroism of light - Now, we address the formulation of the Chern number in terms of the light responses of the CI to circularly polarized light with different polarizations [28]. First, resorting to a Bloch sphere argument where the light-matter coupling is defined through the introduction of a time-dependent vector potential in Eq. (2) above [31], we show that topology can be described from the light-matter coupling at the K and K' points only. In fact, by expressing the transition amplitudes from the lower to the upper band in terms

of eigenstates on the Bloch sphere, the depletion rates $\Gamma_{l \rightarrow u}^\pm(\mathbf{k} = \mathbf{K}, \mathbf{K}')$ encode the mass term $|m| = 6\sqrt{3}t_2$ which determines the size of the band gap at the K-points (see Eq. (S47) of [31]). The next-nearest neighbor hopping term $t_2 e^{i\Phi}$ breaks time-reversal symmetry, and leads to different signs of m at the K and K' points, and therefore, to non-trivial topology [2]. Numerically, we verify this observation by considering the depletion rate as derived in Ref. [28] from Fermi's golden rule:

$$\Gamma_{l \rightarrow u}^\pm(\omega_{\mathbf{k}}, \mathbf{k}) = \frac{2\pi}{\hbar} \left(\frac{E}{\hbar\omega} \right)^2 |\mathcal{A}_{l \rightarrow u}|^2 \delta(\epsilon_u^{\mathbf{k}} - \epsilon_l^{\mathbf{k}} - \hbar\omega) \quad (3)$$

and $\Gamma_{l \rightarrow u}^\pm(\omega_{\mathbf{k}}) = \sum_{\mathbf{k} \in \text{BZ}} \Gamma_{l \rightarrow u}^\pm(\omega_{\mathbf{k}}, \mathbf{k})$. Here, the transition amplitude is given by $\mathcal{A}_{l \rightarrow u} = \langle u_{\mathbf{k}} | \frac{1}{i} \frac{\partial \mathcal{H}_0}{\partial k_x} \mp \frac{\partial \mathcal{H}_0}{\partial k_y} | l_{\mathbf{k}} \rangle$, E is the strength of the drive or the electric field in the original basis, $|u_{\mathbf{k}}\rangle$ and $|l_{\mathbf{k}}\rangle$ are the eigenstates corresponding to the lower and upper bands, $\epsilon_{l,u}^{\mathbf{k}}$ their eigenenergies, and the \pm selects the polarization orientation. In Ref. [28], the sum on the momenta \mathbf{k} involves the entire Brillouin zone. We check that we can evaluate the Chern number in the non-interacting Haldane model with the formula at the Dirac points only, and find for the frequency-integrated rates

$$\frac{1}{2} \int_0^\infty d\omega \sum_{\mathbf{k}=\mathbf{K}, \mathbf{K}'} \Gamma_{l \rightarrow u}^+(\omega_{\mathbf{k}}, \mathbf{k}) - \Gamma_{l \rightarrow u}^-(\omega_{\mathbf{k}}, \mathbf{k}) = \rho C \quad (4)$$

with the constant $\rho = 16\pi^3 E^2 \sqrt{3} |t_1|^2 m^{-2}$. In the non-interacting case, C is one in the topological non-trivial phase of the Haldane model and exactly zero otherwise, and is thus the (ground state) Chern number. The prefactor $1/m^2$ comes from Eq. (3) written in terms of E .

Ground state circular dichroism - Related to the mean field ground state, computing the circular dichroism of light for the entire Brillouin zone using Eq. (3) gives the numerical result of Figs. 3a)-3d). Although both Figs. 3a) and 3b) show the same ground state Chern number, the difference between the two reveals the effect of the particle-hole channel ϕ^x . Increasing V renormalizes t_1 . Considering Fig. 3c), the sign flip of the mass term at one K-point at the CDW transition is reflected by regions of blue curve (Γ^+) turning light red (Γ^-).

Stochastic Chern number and light-matter coupling - When V approaches the size of the smallest band gap around the K-points in Fig. 1a), particle-hole pair excitations will start to form. This leads to the formation of a mixed state which is described below through fluctuations of the stochastic variables around their mean values. We consider Eq. (4) and substitute $\mathcal{H}_0 \rightarrow \mathcal{H}^{\text{mf}}$. The auxiliary fields ϕ^r are mathematically Gaussian random variables $P(\phi^r) = (1/\sqrt{2\pi\xi(V)}) \exp(-\frac{1}{2}(\phi^r - \phi_{\text{mf}}^r)^2 \xi^{-1}(V))$ where $\xi(V) = (1/12V)$, and the mean of the Gaussian distribution is given by the mean-field solution ϕ_{mf}^r . Importantly, ϕ^z acts as Semenoff mass term on the Haldane model modifying the band gap at the Dirac points.

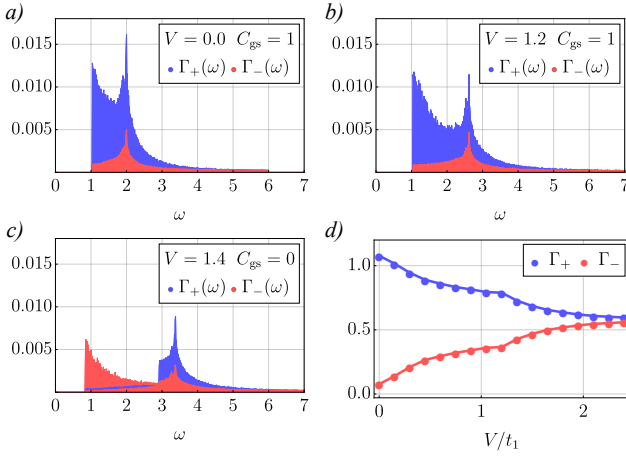


FIG. 3. (color online) (a-c) Ground state depletion rate $\Gamma_{\pm} \equiv \sum_{\mathbf{k} \in \text{BZ}} \Gamma_{l \rightarrow u}^{\pm}(\omega_{\mathbf{k}}, \mathbf{k})$ as a function of frequency for $t_2 = 0.1$ and different fixed values of the interaction strength V . (d) Stochastic frequency-integrated depletion rate $\Gamma_{\pm} \equiv \frac{1}{2} \rho^{-1} \int d\omega \sum_{\mathbf{k}=\mathbf{K}, \mathbf{K}'} \Gamma_{l \rightarrow u}^{\pm}(\omega_{\mathbf{k}}, \mathbf{k})$ as a function of V .

More precisely, sampling ϕ^z around the saddle point solution generates excited states with smaller energy band gaps, see the light red bands in Fig. 1a). We sample the fields $(\phi^x, \phi^y, \phi^z) = \phi$ according to $P(\phi^r)$ while keeping the chemical potential ϕ^0 constant at half-filling. In Fig. 3d), we show the evolution of the ensemble-averaged rates Γ_+ and Γ_- as a function of V , when sampling on the stochastic variables ϕ . These variables are now hidden in the eigenenergies in Eq. (3).

For each configuration we can also compute a ϕ -dependent Chern number $C(\phi)$ via Eq. (4) that will be either one or zero. As the term $3V\phi^z$ plays the role of a Semenoff mass term acting on the Haldane model, we can define - for a given V - ϕ_c^z such that $3V|\phi_c^z| = 3\sqrt{3}t_2$. Then, all states with $|\phi^z| < |\phi_c^z|$ produce a Chern number $C(\phi) = 1$ to C_{st} while all other $|\phi^z|$ contribute zero. Then, we propose to define the *stochastic Chern number*

$$C_{st} \equiv \int_{-\infty}^{+\infty} d\phi P(\phi) C(\phi), \quad (5)$$

which can take non-integer values when it refers to a mixed state. In the limit where $V \rightarrow 0^+$, C_{st} agrees with the definition of the non-interacting topological invariant C . Furthermore, the stochastic variables remain pinned to their ground state values when $V \rightarrow 0^+$, in accordance with $\phi_c^z \rightarrow +\infty$. Computing C_{st} for 10^5 random configurations, as a function of V , then we obtain the result in red in Fig. 4a), which can be compared to the ground state Chern number C_{gs} in blue obtained when $\phi^z = \phi_{mf}^z$. The quantity C_{gs} determines the quantum Hall conductivity, also accessed with iDMRG (see Fig. 2d)). Hence, we can derive C_{st} also via $C_{st} = \int_{-|\phi_c^z|}^{+|\phi_c^z|} d\phi^z P(\phi^z)$ which results in the grey curve in Fig. 4a).

We still observe a correspondence between the ensemble-averaged values of $\Gamma_+ - \Gamma_-$ in Fig. 3d) and

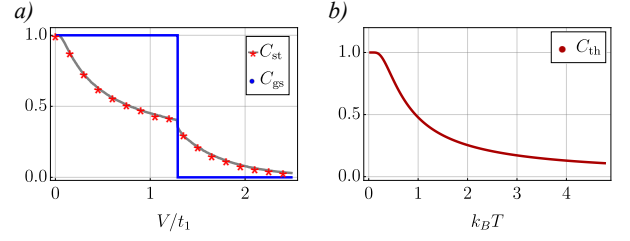


FIG. 4. (color online) (a) Evaluation of the ground state Chern number C_{gs} and stochastic Chern number C_{st} as a function of V . The grey curve comes from an analytical formula. (b) Thermal Chern number C_{th} of the pure Haldane model as defined in Eq. (6) as a function of $k_B T$.

C_{st} as a function of V ; C_{st} still reveals the first-order Mott transition. Allowing the ϕ^r variable to fluctuate around its averaged value, it is then suggestive to make a link to a situation with finite temperature.

By analogy to the finite-temperature version of the Hall conductivity [30], we introduce a finite-temperature version of Eq. (4)

$$\frac{1}{2} \int_0^{\infty} d\omega \sum_{\alpha, \mathbf{k}=\mathbf{K}, \mathbf{K}'} p^{\mathbf{k}} \Gamma_{\alpha}^{+}(\omega_{\mathbf{k}}, \mathbf{k}) - p^{\mathbf{k}} \Gamma_{\alpha}^{-}(\omega_{\mathbf{k}}, \mathbf{k}) = \rho C_{th} \quad (6)$$

where $p^{\mathbf{k}} = (1 + \exp(\epsilon_{u,l}^{\mathbf{k}}/k_B T))^{-1}$ is the Fermi distribution, k_B is the Boltzmann constant, and the variable α here refers to $\{l \rightarrow u, u \rightarrow l\}$ such that $p^{\mathbf{k}}$ effectively mixes the states of the lower and upper band. In the description of Eq. (3), we take the Fermi occupancies into account through the replacement $E^2 \rightarrow E^2 p^{\mathbf{k}}$, implying that if a state is unoccupied then this state cannot couple to light. We then allow in Eq. (6) for heating of the bulk to contribute to C_{th} [30]. From Eq. (6), we find that at low temperatures ($k_B T \ll m$), the finite-temperature Chern number C_{th} decreases smoothly as $1 - e^{-m/k_B T}$ in Fig. 4 [31]. The correction to C_{th} is then in agreement with the probability of a particle-hole pair to occupy the upper band. In the presence of interactions, we observe that the probability to create a particle-hole pair in the topological phase will be dominated by values of $\phi^z \sim \phi_c^z$, producing a correction (reduction) of C_{st} evolving as $P(\phi^z \sim \phi_c^z) \propto e^{-m^2/(k_B T_{eff})^2}$ with an effective temperature $k_B T_{eff} \propto \sqrt{V}$ in Fig. 4. We deduce that interaction effects, through C_{st} , could be visible in the circular dichroism of light (at finite temperature, to produce a mixed state and ensure the validity of the ensemble-averaged protocol) when $k_B T_{eff} \propto \sqrt{V} > k_B T$. For $k_B T > k_B T_{eff}$, the depletion rates should measure C_{th} .

Conclusion - We have introduced a variational topological mean-field theory to describe interaction effects in the fermionic Haldane model with nearest-neighbor interactions. We have then shown how interaction-induced particle-hole pairs can be described through stochastic variables encoding fluctuations around the mean-field theory. This analysis suggests a relation between heat-

ing and interaction effects which could be studied further through the circular dichroism of light. The method could be generalized in various directions, such as bilayer systems [36] and the Kane-Mele [37] model.

Acknowledgements - We acknowledge discussions with N. Regnault, S. Biermann, M. O. Goerbig, G. Uhrig, C. Weitenberg, N. Goldman, W. Wu, A. Rosch, J. Hutchinson, C. Repellin, and L. Herviou. This research was funded by the Deutsche Forschungsgemeinschaft (DFG, German Research Foundation) via Research Unit FOR 2414 under project number 277974659 (PWK and KLH). Furthermore, KLH acknowledges funding from the French ANR BOCA and from CIFAR in Canada. AGG is supported by the ANR JCJC ANR-18-CE30-0001-01.

-
- [1] K. v. Klitzing, G. Dorda, and M. Pepper, *Phys. Rev. Lett.* **45**, 494 (1980).
- [2] F. D. M. Haldane, *Phys. Rev. Lett.* **61**, 2015 (1988).
- [3] C.-X. Liu, S.-C. Zhang, and X.-L. Qi, *Annual Review of Condensed Matter Physics* **7**, 301 (2016).
- [4] J. W. McIver, B. Schulte, F.-U. Stein, T. Matsuyama, G. Jotzu, G. Meier, and A. Cavalleri, *Nature Physics* (2019), 10.1038/s41567-019-0698-y.
- [5] F. D. M. Haldane and S. Raghu, *Phys. Rev. Lett.* **100**, 013904 (2008).
- [6] L. Lu, J. D. Joannopoulos, and M. Soljacic, *Nature Photonics* **8**, 821 (2014).
- [7] M. C. Rechtsman, J. M. Zeuner, Y. Plotnik, Y. Lumer, D. Podolsky, F. Dreisow, S. Nolte, M. Segev, and A. Szameit, *Nature* **496**, 196 (2013).
- [8] J. Koch, A. A. Houck, K. Le Hur, and S. M. Girvin, *Phys. Rev. A* **82**, 043811 (2010).
- [9] K. Le Hur, L. Henriot, A. Petrescu, K. Plekhanov, G. Roux, and M. Schiro, *Comptes Rendus Physique* **17**, 808 (2016).
- [10] T. Ozawa, H. M. Price, A. Amo, N. Goldman, M. Hafezi, L. Lu, M. C. Rechtsman, D. Schuster, J. Simon, O. Zilberberg, and I. Carusotto, *Rev. Mod. Phys.* **91**, 015006 (2019).
- [11] G. Jotzu, M. Messer, R. Desbuquois, M. Lebrat, T. Uehlinger, D. Greif, and T. Esslinger, *Nature* **515**, 237 (2014).
- [12] N. Flaschner, B. S. Rem, M. Tarnowski, D. Vogel, D.-S. Luhmann, K. Sengstock, and C. Weitenberg, *Science* **352**, 1091 (2016).
- [13] C. N. Varney, K. Sun, M. Rigol, and V. Galitski, *Phys. Rev. B* **82**, 115125 (2010).
- [14] I. Vasić, A. Petrescu, K. Le Hur, and W. Hofstetter, *Phys. Rev. B* **91**, 094502 (2015).
- [15] C. N. Varney, K. Sun, M. Rigol, and V. Galitski, *Phys. Rev. B* **84**, 241105 (2011).
- [16] L. Wang, H. Shi, S. Zhang, X. Wang, X. Dai, and X. C. Xie, “Charge-density-wave and topological transitions in interacting haldane model,” (2010), arXiv:1012.5163 [cond-mat.str-el].
- [17] E. Alba, J. K. Pachos, and J. J. García-Ripoll, *New Journal of Physics* **18**, 033022 (2016).
- [18] C. Hickey, P. Rath, and A. Paramekanti, *Phys. Rev. B* **91**, 134414 (2015).
- [19] J. Maciejko and A. Rüegg, *Phys. Rev. B* **88**, 241101 (2013).
- [20] D. Prychynenko and S. D. Huber, *Physica B: Condensed Matter* **481**, 53 (2016).
- [21] J. Imriška, L. Wang, and M. Troyer, *Phys. Rev. B* **94**, 035109 (2016).
- [22] T. I. Vanhala, T. Siro, L. Liang, M. Troyer, A. Harju, and P. Törmä, *Phys. Rev. Lett.* **116**, 225305 (2016).
- [23] S. Rachel, *Reports on Progress in Physics* **81**, 116501 (2018).
- [24] H. J. Schulz, “Functional integrals for correlated electrons,” (1994), arXiv:cond-mat/9402103 [cond-mat].
- [25] G. W. Semenoff, *Phys. Rev. Lett.* **53**, 2449 (1984).
- [26] P. W. Anderson, P. A. Lee, M. Randeria, T. M. Rice, N. Trivedi, and F. C. Zhang, *J Phys. Condens. Matter* **16**, R755 (2004).
- [27] V. L. Ginzburg and L. D. Landau, *Zh. Eksp. Teor. Fiz.* **20**, 1064 (1950).
- [28] D. T. Tran, A. Dauphin, A. G. Grushin, P. Zoller, and N. Goldman, *Science Advances* **3**, e1701207 (2017).
- [29] L. Asteria, D. T. Tran, T. Ozawa, M. Tarnowski, B. S. Rem, N. Fläschner, K. Sengstock, N. Goldman, and C. Weitenberg, *Nature Physics* **15**, 449 (2019).
- [30] A. Rivas, O. Viyuela, and M. A. Martin-Delgado, *Phys. Rev. B* **88**, 155141 (2013).
- [31] In the supplemental material, we provide further information on the lattice structure, the path integral calculation, variational mean-field theory, the energetic and Ginzburg-Landau analysis, the circular dichroism of light at the Dirac points, and further details on the iDMRG computation.
- [32] A. Altland and B. D. Simons, *Condensed Matter Field Theory*, 2nd ed. (Cambridge University Press, 2010).
- [33] D. Zheng, G.-M. Zhang, and C. Wu, *Physical Review B* **84** (2011), 10.1103/physrevb.84.205121.
- [34] J. Hauschild and F. Pollmann, *SciPost Phys. Lect. Notes* , 5 (2018).
- [35] A. G. Grushin, J. Motruk, M. P. Zaletel, and F. Pollmann, *Phys. Rev. B* **91**, 035136 (2015).
- [36] P. Cheng, P. W. Klein, K. Plekhanov, K. Sengstock, M. Aidelsburger, C. Weitenberg, and K. Le Hur, *Phys. Rev. B* **100**, 081107 (2019).
- [37] C. L. Kane and E. Mele, *Phys. Rev. Lett.* **95**, 226801 (2005).
- [38] P. Coleman, *Introduction to Many-Body Physics* (Cambridge University Press, 2015).
- [39] R. Agra, F. v. Wijland, and E. Trizac, *European Journal of Physics* **27**, 407 (2006).
- [40] J. J. Binney, N. J. Dowrick, A. J. Fisher, and M. Newman, *The Theory of Critical Phenomena: An Introduction to the Renormalization Group* (Oxford University Press, Inc., New York, NY, USA, 1992).
- [41] P. Hohenberg and A. Krekhov, *Physics Reports* **572**, 1 (2015).
- [42] S. R. White, *Phys. Rev. B* **48**, 10345 (1993).
- [43] M. P. Zaletel, R. S. K. Mong, and F. Pollmann, *Journal of Statistical Mechanics: Theory and Experiment* **2014**, P10007 (2014).
- [44] J. A. Kjäll, M. P. Zaletel, R. S. K. Mong, J. H. Bardarson, and F. Pollmann, *Phys. Rev. B* **87**, 235106 (2013).
- [45] J. Motruk, A. G. Grushin, F. de Juan, and F. Pollmann, *Phys. Rev. B* **92**, 085147 (2015).
- [46] C. Repellin, Y.-C. He, and F. Pollmann, *Phys. Rev. B* **96**, 205124 (2017).

HONEYCOMB LATTICE STRUCTURE AND NOTATION

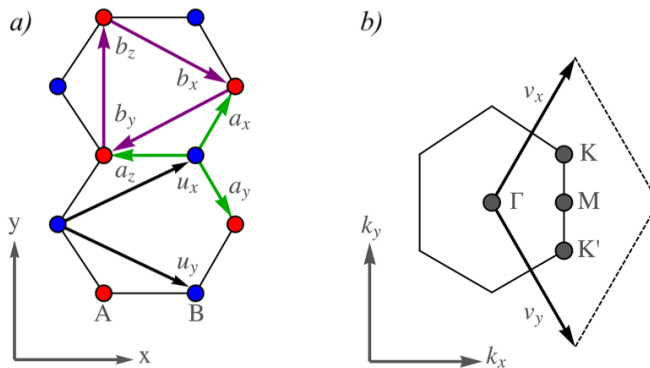


FIG. 5. (color online) (a) Honeycomb lattice in real space with sublattices A and B, lattice vectors, and (next-) nearest neighbor displacements. (b) Honeycomb lattice in momentum space, marking the Brillouin zone, reciprocal lattice vectors and high symmetry points.

First of all, we specify our conventions for the honeycomb lattice and our notation used in the main text, see Fig. 5. The set of lattice vectors is given by

$$\mathbf{u}_x = \frac{1}{2} \left(3, \sqrt{3} \right), \quad \mathbf{u}_y = \frac{1}{2} \left(3, -\sqrt{3} \right), \quad \mathbf{u}_z = (0, 0). \quad (7)$$

Here, the bond length has been set to unity in order to simplify the notation. Moreover, the nearest neighbor displacements on the honeycomb lattice are given by the set of vectors

$$\mathbf{a}_x = \frac{1}{2} \left(1, \sqrt{3} \right), \quad \mathbf{a}_y = \frac{1}{2} \left(1, -\sqrt{3} \right), \quad \mathbf{a}_z = \frac{1}{2} \left(-1, 0 \right). \quad (8)$$

We can then express the next-nearest neighbor displacements on the honeycomb lattice in terms of the \mathbf{a}_p as $\mathbf{b}_i = \mathbf{a}_j - \mathbf{a}_k$ where the tuple (i, j, k) is a permutation of the bond-tuple (x, y, z) . As pointed out in previous works [36], the \mathbf{a}_p basis does not yield a Hamiltonian in Bloch form. Rather, we perform a gauge transform the Hamiltonian to a new basis, given by the lattice vectors \mathbf{u}_i , see Fig. 5.

The Brillouin zone of momentum space is visualized in Fig. 5b) and shows the high symmetry M- and K-points of the Brillouin zone. Specifically, the high symmetry Dirac-points are located at

$$\mathbf{K} = \frac{2\pi}{3} \left(1, \frac{1}{\sqrt{3}} \right), \quad \mathbf{K}' = \frac{2\pi}{3} \left(1, -\frac{1}{\sqrt{3}} \right). \quad (9)$$

HUBBARD-STRATONOVICH DECOUPLING OF THE NEAREST NEIGHBOR INTERACTION

In this work, we consider the spinless Haldane honeycomb model at half filling with nearest neighbor interactions. The model Hamiltonian is composed of two parts $\mathcal{H} = \mathcal{H}_0 + \mathcal{H}_V$ which read explicitly

$$\mathcal{H}_0 = - \sum_{\langle i,j \rangle} t_1 c_i^\dagger c_j - \sum_{\langle\langle i,j \rangle\rangle} t_2 e^{\pm i\Phi} c_i^\dagger c_j, \quad \mathcal{H}_V = V \sum_{\langle i,j \rangle} \left(n_i - \frac{1}{2} \right) \left(n_j - \frac{1}{2} \right), \quad (10)$$

where \mathcal{H}_0 is the Haldane honeycomb model in real space with nearest neighbor hopping amplitude t_1 , complex next-nearest neighbor hopping amplitude $t_2 e^{\pm i\Phi}$, and fixed Peierls phase $\Phi = \frac{\pi}{2}$. Furthermore, \mathcal{H}_V denotes the nearest neighbor interaction with interaction strength V .

In order to prepare the decoupling of the quartic interaction term, we can write \mathcal{H}_V exactly as

$$\mathcal{H}_V = V \sum_{i,p} \left(n_i - \frac{1}{2} \right) \left(n_{i+p} - \frac{1}{2} \right) = V \sum_{i,p,r} \eta_r \left(c_i^\dagger \sigma_{i,i+p}^r c_{i+p} \right)^2 - \frac{V}{2} \sum_{i,p} \left(c_i^\dagger c_i + c_{i+p}^\dagger c_{i+p} - \frac{1}{2} \right), \quad (11)$$

where i denotes a unit cell, p runs over the links (x, y, z) , r runs over $(0, x, y, z)$ and σ^r denotes the Pauli matrices acting on sublattice space with basis $(i(A), i + p(B))$. The coefficients η_r need to fulfill the relations

$$\eta_0 = -\eta_z, \quad \eta_x = \eta_y, \quad \frac{1}{4} = \eta_0 - \eta_x. \quad (12)$$

As pointed out in the main text, we need in principle to choose the η_r such that the decoupling scheme incorporates particle-hole channels (i.e. $\eta_{x,y} \neq 0$) that contribute to the total energy. A priori, a generic choice of the η_r that will ultimately minimize the total energy of the effective Hamiltonian correctly, is not obvious. Rather, a choice of coefficients η_r needs to be justified. We can set our definitions such that $\eta^z = \eta^x$, in agreement with the variational approach presented below (The self-consistent equations (32) and (34) will show the same normalization prefactors on the right-hand side of the equal sign). This approach yields the following choice of the η_r .

$$-\eta_0 = \eta_x = \eta_y = \eta_z = -\frac{1}{8}. \quad (13)$$

Let us now write down the partition function and action

$$\mathcal{Z} = \int D(\Psi, \Psi^\dagger) e^{-\mathcal{S}}, \quad \mathcal{S} = \int_0^\beta d\tau \sum_{\mathbf{k}} \Psi_{\mathbf{k}}^\dagger (\partial_\tau + \mathbf{h}_0(\mathbf{k}) \cdot \boldsymbol{\sigma}) \Psi_{\mathbf{k}} + \mathcal{H}_V \quad (14)$$

where we used the spinor basis $\Psi_{\mathbf{k}}^\dagger = (c_{\mathbf{k}A}^\dagger, c_{\mathbf{k}B}^\dagger)$ to write the Haldane model in momentum space with

$$h_0^x(\mathbf{k}) = -t_1 \sum_p \cos(\mathbf{k} \cdot \mathbf{a}_p), \quad h_0^y(\mathbf{k}) = -t_1 \sum_p \sin(\mathbf{k} \cdot \mathbf{a}_p), \quad h_0^z(\mathbf{k}) = -2t_2 \sum_p \sin(\mathbf{k} \cdot \mathbf{b}_p). \quad (15)$$

Decoupling the quartic interaction term \mathcal{H}_V via a Hubbard-Stratonovich transformation for each $r \in \{x, y, z\}$ yields

$$\exp\left(\frac{V}{8} \sum_{i,p} (c_i^\dagger \sigma_{i,i+p}^r c_{i+p})^2\right) = \int D\phi^r \exp\left(-\sum_{i,p} 2V(\phi_{i+p/2}^r)^2 + V\phi_{i+p/2}^r (c_i^\dagger \sigma_{i,i+p}^r c_{i+p})\right), \quad (16)$$

and for $r = 0$

$$\exp\left(-\frac{V}{8} \sum_{i,p} (c_i^\dagger \sigma_{i,i+p}^0 c_{i+p})^2\right) = \int D\phi^0 \exp\left(-\sum_{i,p} 2V(\phi_{i+p/2}^0)^2 + iV\phi_{i+p/2}^0 (c_i^\dagger \sigma_{i,i+p}^0 c_{i+p})\right). \quad (17)$$

Here we introduced for each r an auxiliary field $\phi_{i+p/2}^r$ on each link between lattice sites i (on sublattice A) and $i + p$ (on sublattice B). The fields ϕ^x and ϕ^y are particle-hole channels, ϕ^0 corresponds to a chemical potential and ϕ^z to a staggered chemical potential in sublattice space that captures CDW order, but at the same time acts as a Semenoff mass term on the Haldane model and therefore controls the topological Chern number.

Effective Hamiltonian

We rewrite the decoupled interaction part in Fourier space and obtain the partition function and action

$$\mathcal{Z} = \int D(\Psi, \Psi^\dagger, \phi^0, \phi^x, \phi^y, \phi^z) e^{-\mathcal{S}}, \quad (18)$$

$$\mathcal{S} = \int_0^\beta d\tau \sum_{\mathbf{k}} \Psi_{\mathbf{k}}^\dagger (\partial_\tau + \mathbf{h}_0(\mathbf{k}) \cdot \boldsymbol{\sigma}) \Psi_{\mathbf{k}} + \sum_{\mathbf{k}, \mathbf{q}, p} \Psi_{\mathbf{k}}^\dagger h_V(\mathbf{k}, \mathbf{q}, p) \Psi_{\mathbf{k}} + \sum_{\mathbf{k}, r} 6V\phi_{\mathbf{k}}^r \phi_{-\mathbf{k}}^r, \quad (19)$$

where the interaction density matrix reads

$$h_V(\mathbf{k}, \mathbf{q}, p) = V \begin{pmatrix} e^{-\frac{i}{2}(\mathbf{k}-\mathbf{q}) \cdot \mathbf{a}_p} (i\phi_{\mathbf{k}-\mathbf{q}}^0 + \phi_{\mathbf{k}-\mathbf{q}}^z) - \frac{1}{2} & e^{\frac{i}{2}(\mathbf{k}+\mathbf{q}) \cdot \mathbf{a}_p} (\phi_{\mathbf{k}-\mathbf{q}}^x - i\phi_{\mathbf{k}-\mathbf{q}}^y) \\ e^{-\frac{i}{2}(\mathbf{k}+\mathbf{q}) \cdot \mathbf{a}_p} (\phi_{\mathbf{k}-\mathbf{q}}^x + i\phi_{\mathbf{k}-\mathbf{q}}^y) & e^{\frac{i}{2}(\mathbf{k}-\mathbf{q}) \cdot \mathbf{a}_p} (i\phi_{\mathbf{k}-\mathbf{q}}^0 - \phi_{\mathbf{k}-\mathbf{q}}^z) - \frac{1}{2} \end{pmatrix}. \quad (20)$$

We would like to consider a time-independent, static model and therefore restrict the analysis to the zero frequency contribution. Furthermore, we restrict the discussion to leading contribution in \mathbf{k} -space for which scattering does not change momentum. Hence, we keep only the zero momentum contribution, i.e. $\mathbf{k} - \mathbf{q} = 0$. The action \mathcal{S} now takes the form

$$\mathcal{S} = \sum_{\mathbf{k}} \Psi_{\mathbf{k}}^{\dagger} \left(\mathbf{h}_0(\mathbf{k}) \cdot \boldsymbol{\sigma} + \sum_p h_V(\mathbf{k}, p) \right) \Psi_{\mathbf{k}} + \sum_{\mathbf{k}, r} 6V \phi_{\mathbf{k}}^r \phi_{-\mathbf{k}}^r, \quad (21)$$

where the interaction density matrix now reads

$$h_V(\mathbf{k}, p) = V \begin{pmatrix} -(\phi^0 + \frac{1}{2}) + \phi^z & e^{i\mathbf{k} \cdot \mathbf{a}_p} (\phi^x - i\phi^y) \\ e^{-i\mathbf{k} \cdot \mathbf{a}_p} (\phi^x + i\phi^y) & -(\phi^0 + \frac{1}{2}) - \phi^z \end{pmatrix}. \quad (22)$$

Here we skipped the zero-momentum index of the fields, i.e. $\phi^r \equiv \phi_0^r$, and redefined the chemical potential $-i\phi^0 \rightarrow \phi^0$ such that ϕ^0 is now real for the matrix $h_V(\mathbf{k}, p)$ to be Hermitian (where it was imaginary before the substitution, such that $i\phi^0$ was real).

We set $\mathcal{H}_{\text{mf}}(\mathbf{k}) = \mathbf{h}_0(\mathbf{k}) \cdot \boldsymbol{\sigma} + \sum_p h_V(\mathbf{k}, p)$, and finally arrive at the effective mean field Hamiltonian $\mathcal{H}_{\text{mf}} = \sum_{\mathbf{k}} \Psi_{\mathbf{k}}^{\dagger} \mathcal{H}_{\text{mf}}(\mathbf{k}) \Psi_{\mathbf{k}}$ where the mean field Hamiltonian density in matrix form explicitly reads

$$\mathcal{H}_{\text{mf}}(\mathbf{k}) = \begin{pmatrix} \gamma(\mathbf{k}) - 3V(\phi^0 + \frac{1}{2}) & -g(\mathbf{k}) \\ -g^*(\mathbf{k}) & -\gamma(\mathbf{k}) - 3V(\phi^0 + \frac{1}{2}) \end{pmatrix}, \quad (23)$$

with the functions $\gamma(\mathbf{k})$ and $g(\mathbf{k})$ defined as

$$\gamma(\mathbf{k}) = 3V\phi^z - 2t_2 \sum_p \sin(\mathbf{k} \cdot \mathbf{b}_p), \quad (24)$$

$$g(\mathbf{k}) = [t_1 - V(\phi^x + i\phi^y)] \sum_p (\cos(\mathbf{k} \cdot \mathbf{a}_p) - i \sin(\mathbf{k} \cdot \mathbf{a}_p)). \quad (25)$$

The term $3V\phi^z$ assumes the role of a Semenoff mass term in the Haldane model, whereas the fields ϕ^x and ϕ^y renormalize the nearest neighbor hopping amplitude t_1 .

SELF CONSISTENT MEAN FIELD EQUATIONS FROM A VARIATIONAL APPROACH

Before deriving the self-consistent equations of the mean field Hamiltonian Eq. 23, we provide a general remark on the derivation of self-consistent mean field equations in the context of Hubbard Stratonovich transformations. Consider some general Hamiltonian $\mathcal{H} = \mathcal{H}_t + \mathcal{H}_{Int}$ with a quadratic, kinetic part H_t and a quartic interaction part of the form $H_{Int} = -\sum_{i,j} U_{ij} c_i^{\dagger} c_j^{\dagger} c_j c_i \equiv -\sum_{i,j} n_i U_{ij} n_j$ with interaction matrix U_{ij} . The quartic term can be decoupled by means of a Hubbard-Stratonovich transformation as [24, 32]

$$\exp(n_i U_{ij} n_j) = \int d\phi \exp(-\phi_i U_{ij} \phi_j - 2\phi_i U_{ij} n_j), \quad (26)$$

where we introduced some Gaussian auxiliary variable ϕ . From the partition function and action

$$\mathcal{Z} = \int D(c, c^{\dagger}, \phi) \exp(-\mathcal{S}), \quad \mathcal{S} = \int_0^{\beta} d\tau \sum_{i,j} c_i^{\dagger} (\partial_{\tau} + h_t) c_j + \phi_i U_{ij} \phi_j + 2\phi_i U_{ij} n_j, \quad (27)$$

one then usually [32, 38] computes the self consistent mean field equations via

$$\left\langle \frac{\delta \mathcal{S}}{\delta \phi_i} \right\rangle \stackrel{!}{=} 0, \quad (28)$$

which would yield in the above example

$$0 = \langle U_{ij} \phi_j + 2U_{ij} n_j \rangle, \quad \Rightarrow \quad \phi_j = -2 \langle n_j \rangle. \quad (29)$$

Now, the problem is that this result is not unique. The auxiliary field ϕ can be thought of as gauge field. Essentially, we can make a transformation as $\phi_i \rightarrow \alpha\phi_i$ in Eq. 26 with some factor α to obtain

$$\mathcal{S} = \int_0^\beta d\tau \sum_{i,j} c_i^\dagger (\partial_\tau + h_t) c_j + \alpha^2 \phi_i U_{ij} \phi_j + 2\alpha \phi_i U_{ij} n_j,$$

This yields the self-consistent mean field equation

$$\left\langle \frac{\delta \mathcal{S}}{\delta \phi_i} \right\rangle \stackrel{!}{=} 0, \quad \Rightarrow \quad \phi_j = -\frac{2}{\alpha} \langle n_j \rangle.$$

Hence, the self-consistent mean field equation depends on α and is therefore not gauge independent. The problem arises, as we only minimize the action (or energy) of the decoupled, ϕ -dependent Hamiltonian. Instead, we need to minimize the energy of the decoupled Hamiltonian (which can be seen as a choice of a trial Hamiltonian) with respect to the original, quartic Hamiltonian. This can be done in the following way. Let \mathcal{H}_{mf} be (a choice of) a mean field or trial Hamiltonian and \mathcal{H} the original, full Hamiltonian. Then, we can rewrite formally $\mathcal{H} = \mathcal{H}_{\text{mf}} + (\mathcal{H} - \mathcal{H}_{\text{mf}})$. On the level of the free energy it follows the Bogoliubov inequality [39, 40]

$$\mathcal{F} \leq \mathcal{F}_{\text{mf}} + \langle \mathcal{H} - \mathcal{H}_{\text{mf}} \rangle. \quad (30)$$

The right hand side of the inequality is a function of the mean field parameters and we need minimize it with respect to ϕ . In our case, for the full Hamiltonian \mathcal{H} in Eq. 10 and the mean field Hamiltonian in Eq. 23, we obtain the following set of self-consistent mean field equations

$$\phi^0 = -\frac{1}{2} \left(\langle c_i^\dagger c_i \rangle + \langle c_{i+p}^\dagger c_{i+p} \rangle \right), \quad (31)$$

$$\phi^x = -\frac{1}{2} \left(\langle c_i^\dagger c_{i+p} \rangle + \langle c_{i+p}^\dagger c_i \rangle \right), \quad (32)$$

$$\phi^y = -\frac{1}{2} i \left(-\langle c_i^\dagger c_{i+p} \rangle + \langle c_{i+p}^\dagger c_i \rangle \right), \quad (33)$$

$$\phi^z = -\frac{1}{2} \left(\langle c_i^\dagger c_i \rangle - \langle c_{i+p}^\dagger c_{i+p} \rangle \right), \quad (34)$$

or in short hand notation using Pauli matrices

$$\phi^r = -\frac{1}{2} \langle c_i^\dagger \sigma_{ij}^r c_j \rangle. \quad (35)$$

The real space amplitudes are evaluated as mean over all lattice sites, for instance

$$\langle c_{i+p}^\dagger c_i \rangle = \frac{1}{N_{\text{sites}}} \sum_{\mathbf{k}} e^{i\mathbf{k} \cdot \mathbf{a}_p} \langle c_{\mathbf{k}A}^\dagger c_{\mathbf{k}B} \rangle \quad (36)$$

$$= \frac{1}{N_{\text{sites}}} \sum_{\mathbf{k}} \sum_{\mu', \nu'} e^{i\mathbf{k} \cdot \mathbf{a}_p} \mathcal{M}_{\mathbf{k}A\mu'}^* \mathcal{M}_{\mathbf{k}B\nu'} \langle \gamma_{\mathbf{k}\mu'}^\dagger \gamma_{\mathbf{k}\nu'} \rangle \quad (37)$$

$$= \frac{1}{N_{\text{sites}}} \sum_{\mathbf{k}} \sum_{\lambda} e^{i\mathbf{k} \cdot \mathbf{a}_p} \mathcal{M}_{\mathbf{k}A\lambda}^* \mathcal{M}_{\mathbf{k}B\lambda}. \quad (38)$$

In the first line, we performed a Fourier transform of the creation and annihilation operators in real space. In the second line, we used $\gamma_{\mathbf{k}} = \mathcal{M}_{\mathbf{k}}^\dagger \psi_{\mathbf{k}}$ where $\mathcal{M}_{\mathbf{k}}$ is a unitary matrix that diagonalizes \mathcal{H}_{mf} . The new spinor basis fulfills $\langle \gamma_{\mathbf{k}\mu'}^\dagger \gamma_{\mathbf{k}\nu'} \rangle = \delta_{\mu'\nu'}$ for occupied states. In Eq. 37, μ' and ν' run over all states, whereas λ in Eq. 38 runs only over occupied states.

ENERGETIC ANALYSIS OF THE PHASE TRANSITION AND THE STOCHASTIC APPROACH

As indicated in the main text, we find at the mean field level a jump of the CDW order parameter ϕ^z at the phase transition. More precisely, the size of the jump depends on the next-nearest neighbor hopping amplitude t_2 . In Fig.

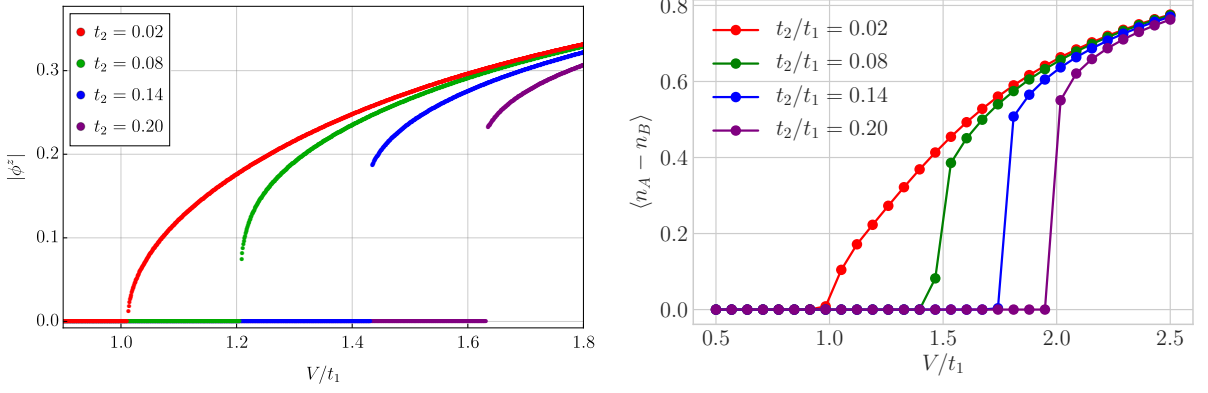


FIG. 6. CDW order parameter from mean field theory (ϕ^z , left) and iDMRG ($L_y = 6$, $\chi = 200$, right) as a function of the interaction strength V/t for different values of the next-nearest neighbor hopping amplitude t_2 . In both cases the smaller t_2 the smaller the jump in the order parameter.

6, we show the CDW order parameter as a function of V for different fixed values of t_2 . The jump becomes smaller the smaller t_2 is. Therefore, at the mean field level, a clear indication of a first order phase transition can only be given when t_2 is sufficiently large. The phase transition appears rather *weakly* first order when t_2 is close to zero. In order to confirm a first order phase transition on the mean field level for sufficiently large t_2 , we compute the total energy of system. Let $|\Omega_{\text{mf}}\rangle$ denote the mean field ground state which in general depends on the self-consistently obtained field ϕ^r , i.e. $|\Omega_{\text{mf}}\rangle \equiv |\Omega_{\text{mf}}\rangle_{\phi}$. Then, we compute the energy of the system via $\mathcal{F}(\phi) = \langle \Omega_{\text{mf}} | \mathcal{H} | \Omega_{\text{mf}} \rangle \equiv \langle \mathcal{H} \rangle$ where $\mathcal{H} = \mathcal{H}_0 + \mathcal{H}_V$ is the original Hamiltonian Eq. 10. This calculation involves exactly decomposing the quartic term $n_i n_j = c_i^\dagger c_i c_j^\dagger c_j$ using Wick's theorem [32] as

$$\langle c_i^\dagger c_i c_j^\dagger c_j \rangle = \langle c_i^\dagger c_i \rangle \langle c_j^\dagger c_j \rangle - \langle c_i^\dagger c_j^\dagger \rangle \langle c_i c_j \rangle - \langle c_i^\dagger c_j \rangle \langle c_i^\dagger c_i \rangle. \quad (39)$$

The amplitudes such $\langle c_i^\dagger c_i \rangle$ are then evaluated similarly to the computation leading to Eq. 38. Explicitly computing the energy in both phases around the transition shows that the energy curves cross at the transition line, see Fig. 7a). This indicates a first order transition as the parameter will jump at the transition to the energetically preferable solution.

This can be further confirmed by computing the energy explicitly for small ϕ^z around the saddle-point solution right before the phase transition. The curve obtained, Fig. 7b) shows a typical Mexican hat form [32] with co-existing minima. We build a Ginzburg Landau theory, i.e. an expansion of the free energy curve. Finding appropriately relevant terms until the order $(\phi^z)^6$ is a difficult task here because V is large as well as ϕ^x , and therefore we perform this task numerically. The free energy can be approximated by a polynomial of the form

$$\mathcal{F}(\phi^z) = \mathcal{F}_0 + \alpha(\phi^z)^2 + \beta(\phi^z)^4 + \gamma(\phi^z)^6, \quad (40)$$

where the coefficients fulfill in general [41] $\alpha > 0$, $\beta < 0$, and $\gamma > 0$ to ensure the co-existence of local minima and that the free energy is bounded from below. Explicitly for e.g. the red curve in Fig. 7b), the coefficients turn out to be

$$\mathcal{F}_0 \approx -2.09, \quad \alpha \approx 0.04, \quad \beta \approx -1.50, \quad \gamma \approx 15.64. \quad (41)$$

Note that odd orders of ϕ^z in Eq. 40 are numerically very close to zero.

Furthermore, note that a plot of the energy landscape around a mean field solution such as Fig. 7b) is an important tool to check the validity of the mean field theory. If relevant mean field parameters are omitted, their weight is not correctly adjusted (the parameters η_r introduced above), or the self-consistent equations have not been such that they minimize the total energy of the system, the energy curve will indeed not show a minimum at the saddle point solution.

Finally, we would like to comment on the stochastic approach to the interacting Chern insulator outlined in the main text from the energetic point of view. Allowing the auxiliary mean field parameters ϕ^r to fluctuate around the saddle point solution changes the energy of the quasi state under consideration. We sample the fields $\phi^{x,y,z}$ and for each configuration we can compute the energy of this quasi state with respect to the wave function $|\Omega\rangle \equiv |\Omega(\phi^x, \phi^y, \phi^z)\rangle$.

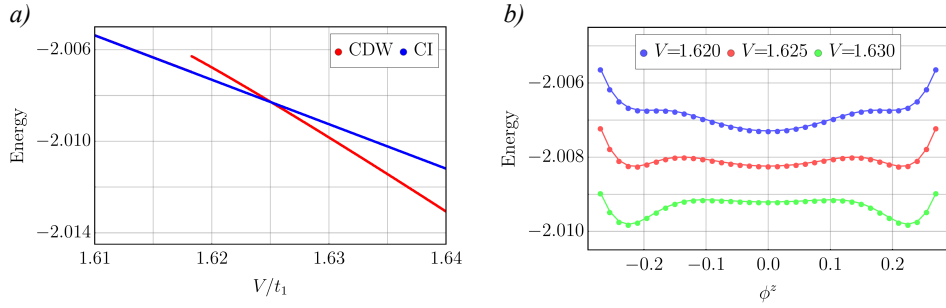


FIG. 7. (color online) (a) Energy of the CI and CDW Mott phases obtained from mean field theory at $t_2 = 0.2$. The curves cut in one point, forcing the CDW order parameter to jump as the system abruptly prefers the change the phase in order to minimize energy. (b) Energy landscape around the mean field solution at $t_2 = 0.2$ in dependence on the CDW order parameter ϕ^z at the phase transition. The coexistence of local minima indicates a first order transition according to Ginzburg-Landau theory.

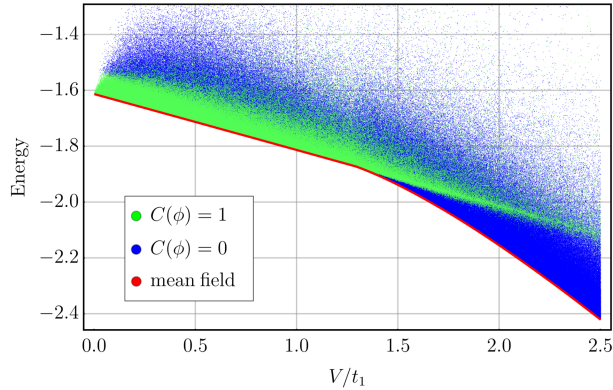


FIG. 8. (color online) Energy of the mean field ground state as function of V (red line). Also shown is the energy distribution of quasi states obtained from sampling $(\phi^x, \phi^y, \phi^z) = \phi$ around the saddle point. This creates quasi-excited states that lie at higher energies than the mean field ground state. Each quasi-state can be attributed a Chern number $C(\phi)$ which will be either one (green) or zero (blue).

Repeating this procedure for 10^3 sampled configurations of the $\phi^{x,y,z}$ for each respective V yields Fig. 8. The red line gives the energy of the mean field ground state which is the lowest energy state for each V . Sampling the ϕ^p fields will result a quasi state at a higher energy. Each quasi state can be associated with a Chern number of either one or zero (depending on ϕ^z). For small V , the mean field ground state (red line) as well as states close to it have Chern number zero. Close to the phase transition, it then becomes more likely to create a state with Chern number zero when moving away from the saddle point. At the phase transition, the ground state acquires Chern number 0 and for further increasing V it becomes more and more unlikely to create an excited state with non-trivial topology.

CIRCULAR DICHROISM OF LIGHT AT THE DIRAC POINTS

Here, we show how the information on the topological properties of the system when coupling circularly to light can be obtained at the Dirac points. For this purpose, we address the Bloch sphere geometry. We also discuss the effect of temperature. We start from the 2×2 matrix form for the Hamiltonian:

$$\mathcal{H}_0(\mathbf{k}) = \begin{pmatrix} \gamma(\mathbf{k}) & -g(\mathbf{k}) \\ -g^*(\mathbf{k}) & -\gamma(\mathbf{k}) \end{pmatrix}, \quad (42)$$

which is the pure Haldane model with no mean field parameters ϕ^r . Its energy eigenvalues read

$$(\epsilon_u^{\mathbf{k}}, \epsilon_l^{\mathbf{k}}) = \pm \sqrt{\gamma^2(\mathbf{k}) + |g(\mathbf{k})|^2} \equiv \pm \epsilon^{\mathbf{k}}, \quad (43)$$

where the positive sign refers to the upper band and the minus sign to the lower band. In analogy with a spin-1/2 Hamiltonian described by a polar angle θ and azimuthal angle φ we can parametrize the Hamiltonian as

$$\frac{\gamma(\mathbf{k})}{\epsilon^{\mathbf{k}}} = \cos \theta, \quad -\frac{g^*(\mathbf{k})}{\epsilon^{\mathbf{k}}} = e^{i\varphi} \sin \theta. \quad (44)$$

From quantum mechanics and the definition of eigenstates of a spin-1/2 particle, the two eigenstates $|u\rangle$ and $|l\rangle$ referring to upper and lowest bands respectively, take the form

$$|u\rangle = e^{-i\varphi/2} \cos(\theta/2) |a\rangle + e^{i\varphi/2} \sin(\theta/2) |b\rangle, \quad (45)$$

$$|l\rangle = -e^{-i\varphi/2} \sin(\theta/2) |a\rangle + e^{i\varphi/2} \cos(\theta/2) |b\rangle. \quad (46)$$

Here, the kets $|a\rangle$ and $|b\rangle$ refer to the states acting on sublattice A and sublattice B , respectively, for a given wavevector. At the two Dirac points, we have $g(\mathbf{K}/\mathbf{K}') = 0$ and $\epsilon_u(\mathbf{K}) = +m/2 = -\epsilon_u(\mathbf{K}')$ with say $m > 0$. Similarly, we have the important mass identifications for the lower band $\epsilon_l(\mathbf{K}) = -m/2 = -\epsilon_l(\mathbf{K}')$.

For the light-matter coupling, here we use a formulation written in terms of the vector potential. Using the spin Pauli matrix representation then this is analogous to the modification in the Dirac Hamiltonian $(\mathbf{p} + \mathbf{A}e/c) \cdot \boldsymbol{\sigma}$ where we set e and c to unity. In the circular basis, the vector potential is defined as $\mathbf{A} = A_0 e^{-i\omega t} (\mathbf{e}_x \mp i\mathbf{e}_y)$ where \mathbf{e}_x and \mathbf{e}_y are unit vectors associated with the x and y directions. The signs in $(\mathbf{e}_x \mp i\mathbf{e}_y)$ refer to right-handed (+) and left-handed (-) polarizations respectively. With such definitions, we obtain the light-matter Hamiltonian:

$$\delta\mathcal{H} = \delta\mathcal{H}_{\pm} = A_0 e^{\pm i\omega t} |a\rangle\langle b| + h.c. \quad (47)$$

This is also equivalent to

$$\delta\mathcal{H} = A_0 \cos(\omega t) (|a\rangle\langle b| + |b\rangle\langle a|) \mp \frac{A_0}{i} \sin(\omega t) (|a\rangle\langle b| - |b\rangle\langle a|). \quad (48)$$

To obtain these equations, we have considered the real parts of the vector potential components $A_x(t)$ and $A_y(t)$ to ensure that the Hamiltonian is hermitian. The speed at the Dirac points is absorbed in A_0 within this notation for $t_2 < 0.2t_1$. Within this formulation, changing the sense of circulation for light is equivalent to change $\omega \rightarrow -\omega$, and the subscript \pm refers to a Jones polarization of light. We can then rewrite $\delta\mathcal{H}$ in the band basis (which diagonalizes the Hamiltonian), and we obtain two classes of terms which can be then studied by mapping the Brillouin zone onto the Bloch sphere

$$\delta\mathcal{H} = A_0 \sin(\theta) \cos(\omega t \pm \varphi) (|u\rangle\langle u| - |l\rangle\langle l|) + A_0 (e^{\pm i\omega t} e^{i\varphi} \cos^2(\theta/2) - \sin^2(\theta/2) e^{\mp i\omega t} e^{-i\varphi}) (|u\rangle\langle l| + h.c.). \quad (49)$$

The first term produces a time-dependent shift of the chemical potential in the original Haldane model, and therefore to ensure the validity of the topological phase, we require that A_0 is small such that the chemical potential still lies in the band gap.

Now, we can apply Fermi's golden rule argument for the inter-band transitions leading to the depletion rate Γ_+ of the lower band defined as

$$\Gamma_+(\mathbf{k}) = \frac{2\pi}{\hbar} |\langle u|\delta\mathcal{H}|l\rangle|^2 \delta(\epsilon_u^{\mathbf{k}} - \epsilon_l^{\mathbf{k}} - \hbar\omega). \quad (50)$$

The (dominant) time-independent terms then give:

$$\Gamma_+(\mathbf{k}) = \frac{2\pi}{\hbar} A_0^2 \frac{1}{2} (1 + \cos^2(\theta)) \delta(\epsilon_u^{\mathbf{k}} - \epsilon_l^{\mathbf{k}} - \hbar\omega), \quad (51)$$

corresponding to a rotating wave approximation. The time-dependent corrections average to zero if one considers a time-Floquet average of the rates or if one goes to the rotating-wave basis.

The important point within this simple argument is that if we change the polarization of light, only the sign of $\hbar\omega$ is changing in the energetic conservation law since by definition $\mathcal{H}_+(\omega) = \mathcal{H}_-(-\omega)$. Therefore,

$$\Gamma_-(\mathbf{k}) = \frac{2\pi}{\hbar} A_0^2 \frac{1}{2} (1 + \cos^2(\theta)) \delta(\epsilon_u^{\mathbf{k}} - \epsilon_l^{\mathbf{k}} + \hbar\omega). \quad (52)$$

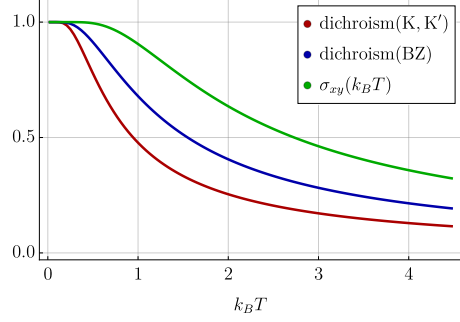


FIG. 9. (color online) Finite temperature version of the topological index. Green: definition from Ref. [30] as in Eq. 55. Blue: based on Eq. 56. Red: Circular dichroism of light as presented in Ref. [28], with a momentum-integral over the entire Brillouin zone.

Below, we perform an analysis around the two Dirac points \mathbf{K} and \mathbf{K}' . We obtain:

$$\sum_{\mathbf{k}=\mathbf{K},\mathbf{K}'} \Gamma_+(\mathbf{k}) - \Gamma_-(\mathbf{k}) = \frac{2\pi}{\hbar} A_0^2 [\delta(m - \hbar\omega) + \delta(-m - \hbar\omega) - \delta(-m + \hbar\omega) - \delta(m + \hbar\omega)]. \quad (53)$$

At these particular points, the form factors simplify since $\cos^2(\theta) = 1$ and the conservation of energy becomes also simple to tackle analytically since it involves the mass gap at the Dirac points. This then leads to

$$\Delta\Gamma = \int_0^{+\infty} d\omega \sum_{\mathbf{k}=\mathbf{K},\mathbf{K}'} \frac{\Gamma_+(\mathbf{k}) - \Gamma_-(\mathbf{k})}{2} = \frac{2\pi}{\hbar^2} A_0^2 \nu, \quad (54)$$

where we can formally rewrite the integral over positive frequencies ω as integral over all frequencies from $-\infty$ to $+\infty$ by including the heaviside step function. This yields only two of the δ functions in Eq. 53 to be non-zero when integrated. In particular, note that $\Gamma_+(\mathbf{K}, -\omega) = \Gamma_-(\mathbf{K}, \omega)$ and $\Gamma_-(\mathbf{K}', -\omega) = \Gamma_+(\mathbf{K}', \omega)$. In Eq. 54 we included a number ν which is exactly one in the topological case where mass inversion is in place at the two Dirac points and zero otherwise.

Here, the quantized response at the Dirac points come from the fact that on the Bloch sphere, the geometrical factor $(1 + \cos^2(\theta))/2 = 1$ at the north and south poles. It is however relevant to comment that this form factor involving the angle θ is not directly equal to the Berry curvature on the sphere. The reason is as follows. For the circular dichroism of light, the sum on the wave-vectors is also attached to the energy conservation encoded in the delta-function in the definitions of Γ_+ and Γ_- . Therefore, performing the sum over wave-vectors on the sphere, *i.e.* integrating on the angles θ and φ is more complicated than performing a direct calculation in the Brillouin zone. Our key observation here is that we can simply consider the two Dirac points, *i.e.* the south and north poles on the sphere encoding the mass effects in the topological Haldane model, to reproduce a quantized light response as found in Ref. [28]. In this sense, ν in the formula above can be then identified as the Chern number C introduced in the Letter.

FINITE TEMPERATURE VERSION OF THE TOPOLOGICAL INDEX

In Ref. [30], a finite temperature version of the Hall conductivity was introduced as

$$\sigma_{xy}(k_B T) h/e^2 = \sum_{\alpha \in \{u,l\}} \int_{\mathbf{k} \in \text{BZ}} d\mathbf{k} p^{\mathbf{k}}(k_B T) F_{x,y}^{\alpha}(\mathbf{k}) \quad (55)$$

with the Fermi distribution $p^{\mathbf{k}}(\epsilon_{u,l}^{\mathbf{k}}) = (\exp(\epsilon_{u,l}^{\mathbf{k}}/k_B T) + 1)^{-1}$. Here, the factor $p^{\mathbf{k}}$ effectively mixes upper and lower band states. Hence, Eq. 55 will yield a topological index one for zero temperature and a many-body topological index that approaches zero in the limit of large temperatures, see Fig. 9. Furthermore note, that Eq. 55 takes heating effects from the bulk into account such that even in a zero-temperature trivial phase, Eq. 55 will yield a many-body Hall conductivity larger than zero for $T > 0$ [30].

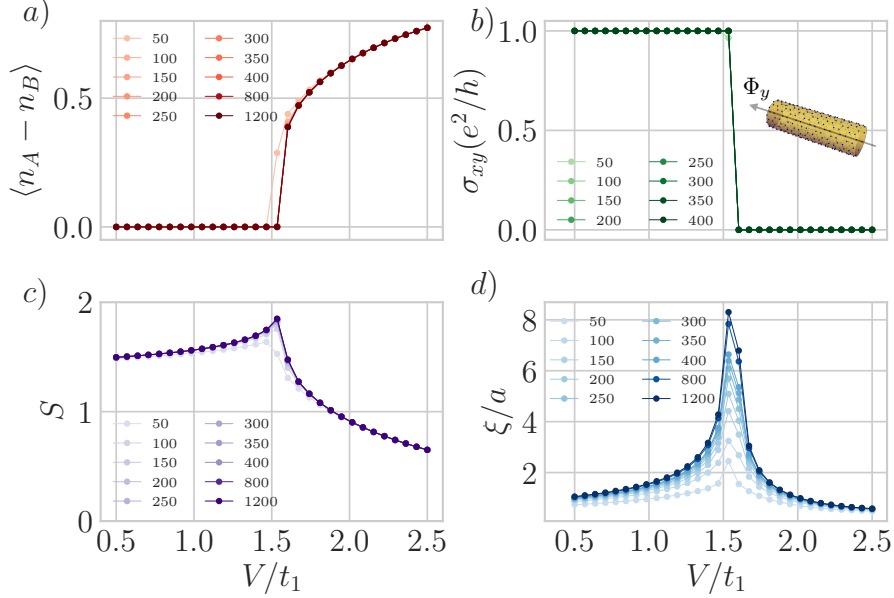


FIG. 10. iDMRG convergence. In a) the figure shows the correlation length ξ/a in units of the lattice constant a . b) shows the Hall conductivity calculated by adiabatically threading a flux $\Phi_y/\Phi_0 \in [0, 2\pi]$ in units of the flux quantum Φ_0 through the cylinder geometry (inset). Within the Chern insulator or CDW phase one or zero charges are pumped leading to $\sigma_{xy} = e^2/h$ or $\sigma_{xy} = 0$ respectively. c) shows the entanglement entropy S and d) the charge density wave order parameter. Except for σ_{xy} which converges at $\chi = 100$, these quantities are calculated for bond dimensions $\chi \in [50, 1200]$ and convergence is achieved for $\chi \sim 200$.

For the circular dichroism of light, we can produce a similar finite temperature version as in Ref. [30] such that the finite temperature version of Eq. 54 reads

$$\int_0^{+\infty} d\omega \sum_{\mathbf{k}=\mathbf{K}, \mathbf{K}'} \sum_{\alpha=l \rightarrow u, u \rightarrow l} \frac{p^{\mathbf{k}} \Gamma_{\alpha}^{+}(\mathbf{k}) - p^{\mathbf{k}} \Gamma_{\alpha}^{-}(\mathbf{k})}{2}. \quad (56)$$

Note that Eq. 55 and Eq. 56 yield in principle the same result, however the finite temperature topological index scales slightly differently with $k_B T$. Also a finite temperature version of the circular dichroism that integrates over the entire Brillouin zone shows a different scaling behavior, see Fig. 9.

Taking into account that at very low temperatures

$$(1 + \exp(-\epsilon^{\mathbf{k}}/k_B T))^{-1} \approx 1 \quad \text{and} \quad (1 + \exp(\epsilon^{\mathbf{k}}/k_B T))^{-1} \approx \exp(-\epsilon^{\mathbf{k}}/k_B T), \quad (57)$$

then we obtain that in the formula above, ν would acquire $-\mathcal{O}(e^{-m/k_B T})$ corrections in agreement with the Arrhenius law for the distribution of particle-hole pairs in the upper band at finite temperature. Here, the new physics comes from when $k_B T$ (or the interaction V) becomes of the order of the mass m . Pushing the validity of the corrections to the limit where $k_B T \gg m$, now we see that ν should behave as $m/k_B T$ for large temperatures.

DMRG COMPUTATIONAL DETAILS

In this section we give further details of our infinite density matrix renormalization group results (iDMRG). All our results are computed using the open source package TENPY [34], which implements the iDMRG algorithm [42] in the language of matrix-product states. The bond dimension χ sets the maximum linear dimension of the matrices that are stored to represent a given ground-state, and determines the accuracy of the method. For a given χ the variational algorithm determines the ground-state of the system in the infinite cylinder geometry, which uses translational invariance to reach system sizes of $[L_y, \infty]$. Our conclusion and the following discussion are based on simulations with cylinder circumferences $L_y = 6, 12$ and $\chi \in [50, 1200]$ which we find sufficient to reach convergence.

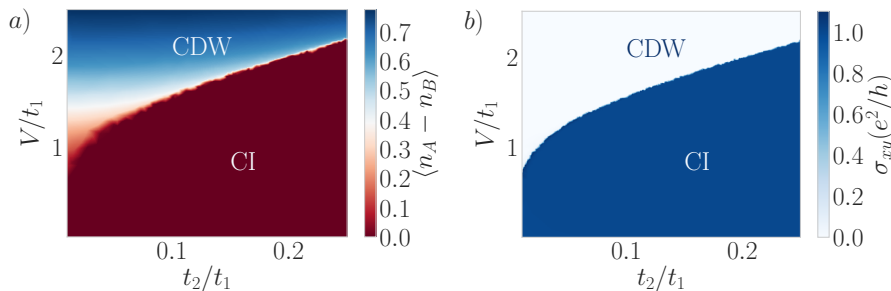


FIG. 11. Phase diagrams. a) CDW order parameter and b) σ_{xy} calculated in iDMRG for $L_y = 6$, $\chi = 200$. The phase boundary for both order parameters fall on top of each other indicating that there is no coexistence of a finite CDW order with a non-zero Hall conductivity.

Finite bond dimension effects and order of the phase transition

For the interacting Haldane hamiltonian given in the main text, we provide representative results in Fig. 10. They are obtained for a cut in the phase diagram for $L_y = 6$ lattice sites and $t_2/t_1 = 0.1$ as a function of V/t_1 . We show the CDW order parameter, the Hall conductivity σ_{xy} , the entanglement entropy S , and correlation length ξ/a in units of the lattice constant a of the ground-state wave-function with different $\chi \in [50, 1200]$. We compute the CDW order parameter through the ground-state expectation values of the difference of the two sub-lattice densities $\langle n_A - n_B \rangle$. The entanglement entropy S is computed by cutting the system in real space and computing the Schmidt decomposition of the groundstate, and relating the corresponding Schmidt eigenvalues to the entanglement entropy [34]. The correlation length ξ is defined as the largest decay of correlation functions, which is set by the second largest eigenvalue of the transfer matrix [34]. Finally, to obtain the Hall conductivity σ_{xy} we use the method of adiabatic flux insertion implemented numerically as detailed in Refs. [35, 43]. It consists of threading a magnetic flux through the axis of the cylinder by twisting the boundary conditions by a phase Φ_y (see inset in Fig. 10b)). As the flux is threaded from 0 to 2π in units of the flux quantum Φ_0 , we monitor the pumped charge through a given real-space cut of the cylinder. One charge pumped in such a cycle is equivalent to $\sigma_{xy} = e^2/h$ while no charge pumped amounts to $\sigma_{xy} = 0$ [35].

In Fig. 10 we observe that all quantities within the CI and CDW phases do not change significantly above $\chi \sim 200$, a size for the bond dimension that is consistent with previous work [35]. The topological origin of the Hall conductivity allows it to converge faster even close to the phase transition, and we find it fully converged at $\chi \sim 100$. The inverse gap in the CDW and Chern insulator phases determines the largest length scale up to which correlations spread. Thus the convergence is better as the parameters are chosen deeper in these phases, where the gap is expected to be larger, and the correlation length shorter, consistent with Fig. 10a).

In Fig. 11 we show the CDW and σ_{xy} phase diagrams for $\chi = 200$. The two phase boundaries coincide for this range of parameters; we find no intermediate phase. Although extracting the nature of the phase transition is a subtle issue in iDMRG data there are hints that this transition is first order. First, both the CDW order parameter and σ_{xy} show a clear discontinuity, which can be interpreted as a first order phase transition, consistent with mean field theory. Interestingly, the correlation length ξ does not show such an evident discontinuity. We remind the reader that a second order phase transition presents a divergent correlation length ξ at the transition as a function of increasing bond dimension χ [44]. Moreover, the entanglement entropy of a critical system is expected to scale as $S = c/6 \ln(\xi/a) + s_0$ where c is the central charge and s_0 is a constant [44]. A first order phase transition on the other hand presents either a discontinuity in χ [35, 45], or a saturating behaviour of the maximal or critical correlation length, ξ_c , as a function of χ at the phase transition [46]. Our iDMRG results shown in Fig. 10 point to the latter scenario since the correlation length at the critical point seems to saturate as a function of bond dimension. This is supported by a more careful analysis, shown in Fig. 12, where we plot the maximum correlation length ξ_c as a function of χ (a), and the maximum entanglement entropy S_c as a function of ξ_c in semi-logarithmic scale (b). Both ξ_c and S_c show an increasing yet saturating behaviour, supporting the absence of a critical state with divergent correlation length. Such an increasing but non-divergent correlation length at the transition is sometimes referred to as a weak first order transition.

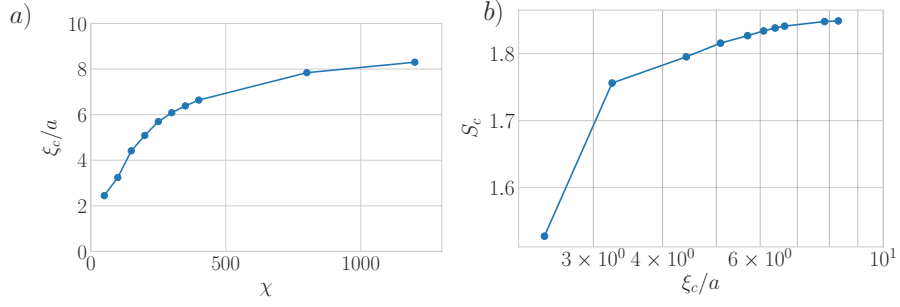


FIG. 12. Order of the phase transition in iDMRG. a) shows the correlation length at the transition ξ_c in units of the lattice constant a . A second order phase transition would show a divergent correlation length at the transition. Instead the correlation length seems to saturate with increasing χ . b) Entanglement entropy at the transition S_c plotted as a function of the correlation length at the transition ξ_c in units of the lattice constant a . The entanglement saturates as a function of correlation length, deviating from the critical scaling law $S_c = c/6 \ln(\xi_c/a) + s_0$.

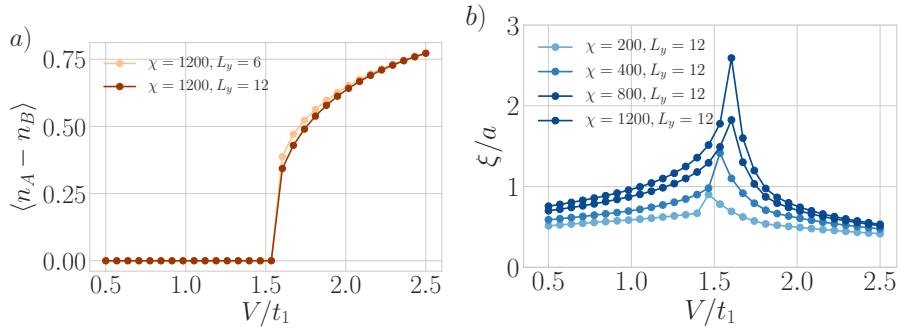


FIG. 13. Fine size effects. We show the CDW order parameter (left) and correlation length in units of the lattice constant (ξ/a , right) calculated in iDMRG for $L_y = 6$ and $L_y = 12$, and $\chi = 1200$. The phase boundary for the CDW order parameter does not change, and the correlation length drops when increasing the system size. These indicate that large system sizes lead to qualitatively the same results.

Finite size effects

To address the robustness of our results we have performed the calculations for $L_y = 12$ with χ up to $\chi = 1200$ (see Fig. 13) for $t_2/t_1 = 0.1$. The results are shown in Fig. 13. Fig. 13a) shows that the CDW transition is still abrupt and occurs at the same value of V/t_1 for larger system sizes. For $L_y = 12$ the correlation length ξ close to the transition presents the same peaked structure but is smaller in magnitude that that of $L_y = 6$ (see Fig. 10d)). The decrease in magnitude of ξ can be interpreted as a sign of an increase in the gap size of both the CDW and Chern insulator phases.